Probing the electronic and geometric structure of ferric and ferrous myoglobins in physiological solutions by Fe K-edge absorption spectroscopy: Supplementary Information

F.A Lima[a,1], T. J. Penfold,[a,b,c], R. M. van der Veen,[a,2], M. Reinhard[a], R. Abela[c], I. Tavernelli[b], U. Rothlisberger[b], M. Benfatto[d], C.J. Milne[a3] and M. Chergui[a]

a) Ecole polytechnique Fédérale de Lausanne, Laboratoire de spectroscopie ultrarapide, ISIC, FSB-BSP, CH-1015 Lausanne, Switzerland

b) Ecole polytechnique Fédérale de Lausanne, Laboratoire de chimie et biochimie computationnelles, ISIC, FSB-BSP, CH-1015 Lausanne, Switzerland

c) Paul Scherrer Institut, CH-5232 Villigen, Switzerland.

d) Laboratori Nazionali di Frascati, Istituto Nazionale di Fisica Nucleare, CP13, 00044 Frascati, Italy.

List of Figures

S1 Schematics of the relevant parameters used in the fits of the Myoglobin XAS using the MXAN code. The heme plane and relative ligand geometry (angles α and β) are shown. Schematics of the parametrisation used in the fits of the Myoglobin XAS using the MXAN code. 5

S2 *Left:* The Q-band region of the absorption spectrum of all forms of myoglobin *Right:* The Soret band region of the absorption spectrum of all forms of myoglobin 8

S3 Calculated XAS spectrum of MbCO as a function of the angle α (a). A zoom into the XANES region is shown in (b) 9

S4 (a) A zoom into the near-edge and the S^2 value (b) for the calculated XAS spectrum of MbCO as a function of the angle α 10

S5 The S^2 value, plotted as a function of energy for the calculated XAS spectrum of MbCO as a function of the angle α 11

S6 Calculated XAS spectrum of MbO_2 as a function of the Fe-O bond length (a) and zoom in the region around the edge (b). (c) The S^2 value for the difference Fe-O bond lengths. 13

S7 MXAN best fit of the XAS spectrum of metMb with (a) and without (b) a water molecule in the position of the ligand. 15

[1]Present Address: Centro Nacional de Pesquisa em Energia e Materiais, Laboratrio Nacional de Luz Sncrotron, Rua Giuseppe Mximo Scolfaro, Campinas, SP, Br.

[2]Present Address: Arthur Amos Noyes Lab Chem Phys, Phys Biol Ctr Ultrafast Sci and Technol, Pasadena, CA 91125 USA.

[3]Present Address: SwissFEL, Paul-Scherrer-Institut, CH-5232 Villigen, Switzerland.

List of Tables

S1 Table with the non-structural parameters used in the MXAN fits of the different myoglobin XAS spectra. 7
S2 Model optimised structure of MbCO 16
S3 Model optimised structure of MbNO. 17
S4 Model optimised structure of MbO_2. 18
S5 Model optimised structure of MbCN. 19
S6 Model optimised structure of metMb. 20
S7 Model optimised structure of deoxyMb. 21

S1 Experimental Methods

S1.1 Sample preparation and handling

•*Unligated ferric Myoglobin (metMb)*: The preparation of unligated ferric myoglobin (metMb) solutions is straightforward. The Mb lyophilized powder is already in the oxidized form and no special care is required to avoid contact with oxygen. It is sufficient to dissolve the lyophilized powder in sodium phosphate buffer at the desired concentration. For all forms of Mb presented here, we used solutions of 4 mM concentration.

•*Carboxy-Myoglobin (MbCO)*: We start off from a metMb solution, which is then saturated with carbon monoxide by bubbling CO gas through the solution for at least 15 minutes. The next step is to add a five-fold molar amount of $Na_2S_2O_4$ dissolved in degassed sodium buffer to reduce to iron atom from Fe^{III} to Fe^{II}. The MbCO sample was kept under a CO atmosphere to ensure sample integrity.

•*Nitrosyl-Myoglobin (MbNO)*: There are two different ways of preparing MbNO and the resulting protein crystal structure depends on the preparation method [1]. Our samples were prepared by reacting metMb with nitrite/dithionite in the absence of oxygen, according to the procedure by Kim et al. [2]. A solution of 4 mM myoglobin (metMb) was mixed with 33.3 mM solution of $NaNO_2$. The latter was prepared using commercially-available $NaNO_2$ dissolved in degassed buffer and kept under N_2 atmosphere. The sample was kept under Nitrogen atmosphere at all times to prevent oxidation and the slow exchange of NO by the oxygen of the air.

•*Oxy-Myoglobin (MbO_2)*: The same procedure as for MbCO was followed except that the CO gas was substituted by a gas mixture of 40% oxygen in helium. The MbO_2 preparation was stable for >5 hours, which is sufficient to complete all the measurements.

•*Cyano-Myoglobin (MbCN)*: We added cyanide (CN) to a solution of metMb. The former was derived from a solution of NaCN in basic environment (pH ∼14) to prevent the formation of CN gas when it encounters water.

•*Unligated ferrous Myoglobin (deoxyMb)*: The unligated ferrous Myoglobin (deoxyMb), is obtained by adding sodium dithionite ($Na_2S_2O_4$), dissolved in the previously degassed buffer, in slight excess

to a solution of metMb. In addition, this state is very unstable and requires extra care during the experiments in order to avoid contact with the oxygen present in air, which results in a rapid transformation into MbO_2.

All the solvents used were degassed by bubbling high-purity nitrogen gas for at least 10 hours. The changes upon ligand substitution were monitored by the corresponding changes on the UV-Vis spectrum. The UV-Vis spectra were monitored during the course of the XAS experiments and no changes were identified, indicating the Mb integrity was preserved during the experiments.

The Mb sample preparation was performed inside closed bottles under nitrogen atmosphere (except the carboxy-myoglobin and oxy-myoglobin which were kept at CO and a mixture of He and O_2 atmospheres, respectively). Flexible tubes (PharMed BTP) connected to a quartz capillary were used to circulate the samples using a peristaltic pump. UV-Vis absorption spectra have been used to assess the successful oxidation state change and ligation by comparing the positions of the strongest absorption bands (Soret and Q-bands) with the values reported in the literature [**?**] (see figure S2. The UV-Vis spectra of metMb, deoxyMb, MbNO and MbCO have been monitored throughout the XAS measurements. In the case the UV-Vis spectra have not been measured concomitantly with the XAS experiments (MbO2 and MbCN), aliquots of the samples have been collected and their spectra measured offline. These spectra were equivalent to the ones measured prior to the experiment and also to the ones reported in the literature.

S1.2 Setup for steady state XAS

We used lyophilized powder Mb from equine skeletal muscle (Sigma-Aldrich), with a purity 95-100%, dissolved in a sodium phosphate buffer at pH 7.0. To avoid any uncontrolled contact with oxygen the solvent was degassed by bubbling with nitrogen gas (purity >99.99%) for at least 10 hours prior to use. The solvent was kept in a glass bottle, under a controlled slight overpressure of nitrogen gas, sealed using plastic caps with four apertures. These apertures, from which all the liquid extraction and gas input were performed (using gas-tight syringes) were sealed with silicone disks. The same degassing procedure was used during the XAS experiments, for which two of the silicone disks were replaced by flexible tubes (PharMed BTP) connected to a quartz capillary (Hilgenberg GmbH, 2 mm path length, 10 μm walls) through which the samples were flowed. Additionally, two thin tubes were inserted through one of the silicone disks providing a parallel flow circuit to monitor the visible absorption (UV-Vis) in order to confirm the sample integrity.For all forms of Mb presented here, we used solutions of 4 mM concentration.

The myoglobin XAS spectra were collected at the microXAS beamline at the Swiss Light Source (Paul Scherrer Institut). The x-rays were monochromatized using a double-crystal, fixed exit monochromator (DCM) using a Si(111) crystal pair with an energy resolution of $\sim$ 1 eV. The x-rays were focused down to 500x500 μm^2 employing an x-ray mirror pair in the Kirkpatrick-Baez (KB) geometry. The x-ray energy was calibrated with an iron foil, setting the energy of the first derivative of the XAS spectrum to 7112 eV. The spectra were acquired in total fluorescence yield mode (TFY) using two single-element silicon drift detectors (Ketek, AXAS-SDD10-138500,

10 mm^2 active area) placed at an angle normal to the incoming x-ray beam in order to minimize the elastic scattering during the measurements. On the tip of each fluorescence detector a conical-shaped metal piece was placed so as to improve the contrast between the x-ray fluorescence and the elastic scatter. An integration window of about 150 eV was set around the iron K-α emission line (*ca.* 6404 eV). An ion chamber (Oxford-Danfysik) filled with 1 bar of helium gas was used to monitor the incoming x-ray intensity. The background subtraction and spectra normalization were performed using the ATHENA package [3]. Each spectrum coming from each of the two fluorescence detectors was processed individually prior to averaging, which was necessary in order to improve the signal-to-noise (S/N) ratio.

S2 Theory and Computations

S2.1 Calculation the XANES spectra

The simulations of the post-edge region of the XANES spectrum are carried out using the MXAN code [4–7], which performs a fit by a comparison between experimental data and theoretical simulations. The calculations are performed within the Green's function multiple scattering (MS) formalism, the potential is based upon the muffin-tin (MT) spheres for which the initial radii were chosen according to the Norman criterion [8,9]. In the first step of the optimisation a self-consistent field (SCF) calculation of the potential, including the whole atomic cluster, is performed. This is not recalculated in the following steps because the computational expense makes its use impractical. This can be a source of error in the fitting procedure, especially if the starting structure differs considerably from the real geometry [6, 10]. However, it was recently shown that refining some non-structural parameters related to the MT potential (MT radii overlap, Fermi energy, E_0 and the intestitial potential V_{0inp} according to the extended continuum scheme [7]) at each step of the calculation can partially account for not using SCF potentials at each step [11, 12]. This approach has been successfully applied to the XAS analysis of crystalline heme proteins. [12–15]. The exchange and correlation part of the potential are calculated in the framework of the Hedin-Lundqvist (HL) scheme [9, 16], using only the real part of the complex potential to avoid overdamping of the spectral features at low energies, characteristic of this type of potential [6, 10, 17–19]. All inelastic losses were taken into account by a phenomenological approach in which the calculated cross-section is convoluted with a Lorentzian broadening function having an energy-dependent width given by $\Gamma(E) = \Gamma_c + \Gamma_{mpf}(E)$. The constant part Γ_c accounts for contributions coming from the core hole lifetime and the experimental resolution, while the energy dependent term $\Gamma_{mpf}(E)$ represents all the intrinsic and extrinsic inelastic processes. The parameters of the broadening function are derived via a simulated annealing-like method before the structural calculation starts and are fit by a Monte Carlo search at every minimization step. Recently, the MXAN code modified the way it calculates the losses by introducing a further convolution in the constant term Γ_c [20]. It now includes a convolution with a Gaussian function (Γ_{exp}) to mimic the experimental resolution. Therefore, the contribution coming from the energy-independent Lorentzian (Γ_c) now

accounts only for the core-hole. In this way a more accurate description of the inelastic losses of the photoelectron is achieved.

For each fit, a cluster of radius 7 Å around the Fe atom was used to calculate the potentials. It included the porphyrin ring, the ligand (when present), the proximal (His93) and part of the distal (Hist64) histidines. A scattering radius of 5 Å was used in the FMS, corresponding to 32 to 36 atoms depending on the Mb form. In all cases this value was found to converge the calculation for all of the resonances. All of the simulations used as starting points the crystallographic structures from the Protein Data Bank (PDB), whose numbers are listed in Table S7. These were chosen according to two criteria: a) the preparation method used and b) the highest resolution crystallographic structure.

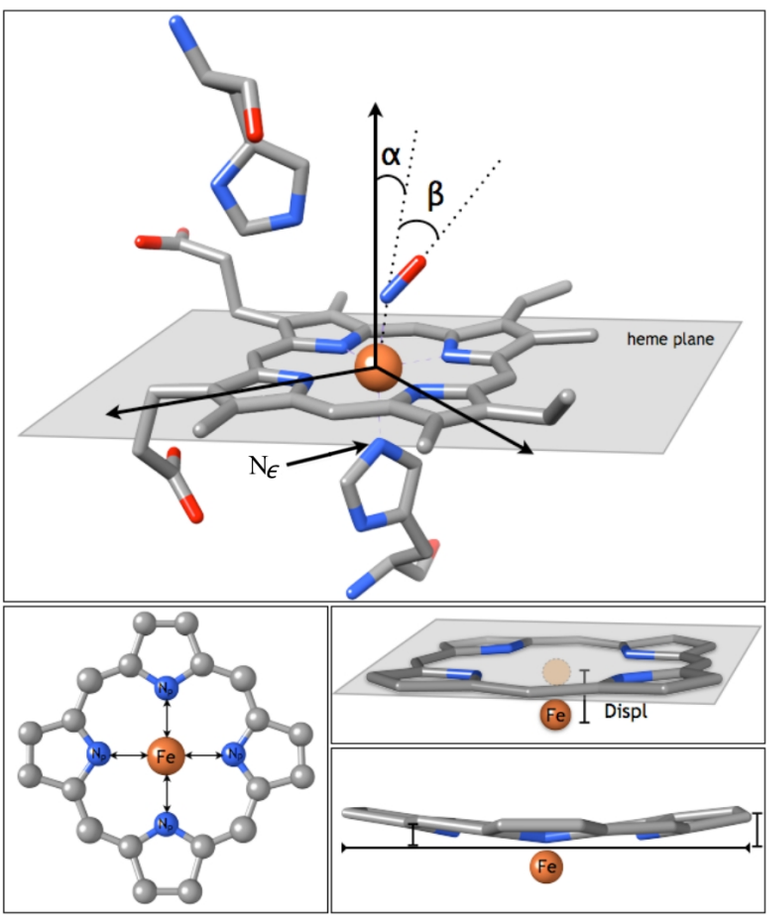

Figure S1: Schematics of the relevant parameters used in the fits of the Myoglobin XAS using the MXAN code. The heme plane and relative ligand geometry (angles α and β) are shown. Schematics of the parametrisation used in the fits of the Myoglobin XAS using the MXAN code.

The fits follow the same philosophy as employed by Della Longa et al. [13]. For a specific

geometry the heme and surrounding atoms are parametrized to minimize the number of structural parameters necessary to describe the heme environment. The set of parameters used to describe the Mb structure (Fig. S1) are described below.

• *Fe-N_p*: The distance between the Fe atom and the nitrogen atoms of the porphyrin ring.

• *Displ*: - The Fe atom displacement out of the heme plane. It moves the Fe atom in absolute values with respect to the average heme plane.

• *Dom1*: - The doming of the porphyrin ring. It moves the four N atoms of the porphyrin ring in a direction perpendicular to the heme plane. It is used only on the case of deoxyMb.

• *Dom2*: - The doming of the porphyrin ring in a similar way as Dom1. It moves the 8 C atoms closest to the Fe in the porphyrin ring in a direction perpendicular to the heme plane (see Figure 1). Likewise, it is used only on the case of deoxyMb.

• *Fe-L1*: - The distance between the Iron atom and the ligand closest atom (e.g. C of the CO molecule or N of NO molecule).

•α: - The angle between the direction perpendicular to the heme plane and the vector defined by the bond between the Fe and the closest atom of the ligand.

•β: - The angle between the vectors defined by the bond between the Fe and the closest atom of the ligand and the one defined by the bond between the two atoms of the ligand.

• *Fe-N_ϵ*: - The distance between the Fe atom and the N_ϵ on the proximal histidine (His93).

• *L1-L2*: - Internuclear distance of the diatomic ligand molecule.

S2.2 Calculation of the pre-edge using TDDDFT

Using the optimised structures, obtained from the MXAN procedure, the pre-edge transitions were calculated using TD-DFT adapted for core hole spectra [21, 22], as implemented within the ORCA quantum chemistry package [23]. The model geometries include the porphyrin ring, the ligand (if present), proximal histidine (His93) and the distal histidine (His64). Hydrogen atoms were added to the structure, using the MacMolPlt package [24] and their positions were optimised using ORCA, keeping the positions of the heavier atoms fixed. The TD-DFT equations, within the approximation of the BP86 [25, 26], or B3LYP* *exchange-correlation* functionals [27, 28] were solved using the Tamm-Dancoff approximation [29]. A CP(PPP) basis set [30] was used for the iron, while the remaining heavy atoms a TZVP basis was used and the hydrogens used a DZP basis set. In each case the interaction with the X-ray field was described using the electric dipole + quadrupole approximation. All of the calculations used a dense integration grid (ORCA Grid4). Following calculation all of the oscillator strengths were convolved with a Lorentzian function having a 2.0 eV FWHM. In addition a shift of 125 eV was also applied to all of the spectra to match the experiment.

S2.3 Supplementary Results

A summary of the fit details of the XANES spectra for each form of myoglobin is shown in Table S1, including the two additional nonstructural parameters, namely E_0 and magnitude of the MT overlap. S^2 is the square residual between the fit and the experimental data. [6]

	PDB file	Γ_c	Γ_{exp}	E_0 (eV)	MT overlap [%]	S^2
MbCO	1A6G	1.42	0.70	7125.0	12	1.99
MbNO	2FRJ	1.47	0.65	7125.3	8	2.22
MbCN	2JHO	1.36	0.60	7127.1	3	2.83
MbO_2	1MBO	1.13	0.70	7126.8	2	0.98
deoxyMb	1BZP	1.59	0.60	7122.6	-3	1.97
metMb	1BZ6	1.52	0.70	7126.2	0	0.57

Table S1: Table with the non-structural parameters used in the MXAN fits of the different myoglobin XAS spectra.

d

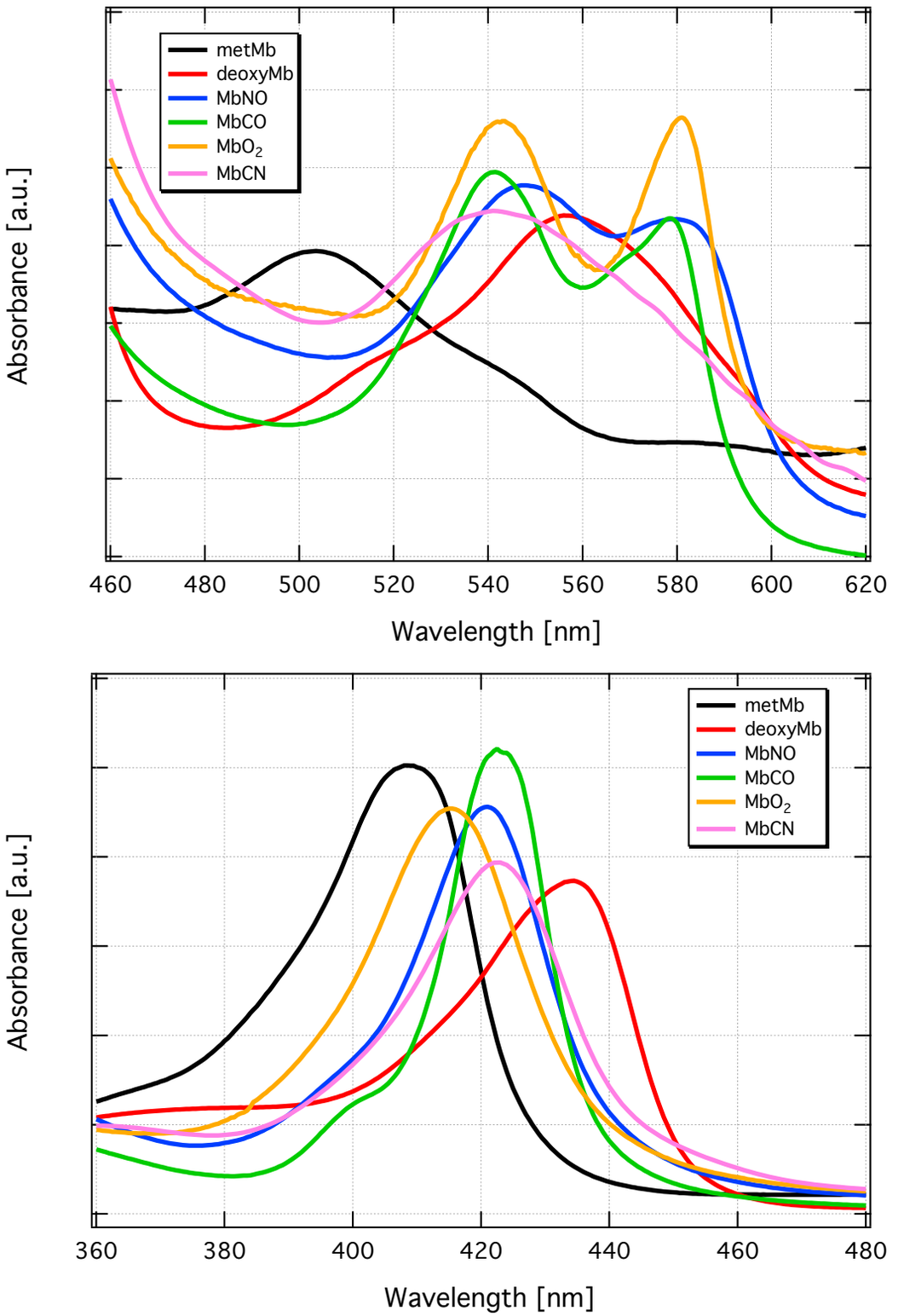

Figure S2: *Left:* The Q-band region of the absorption spectrum of all forms of myoglobin *Right:* The Soret band region of the absorption spectrum of all forms of myoglobin

S2.4 Calculated XAS spectrum of MbCO as a function of the angle α

To investigate the sensitivity of the α angle for the XANES spectrum of MbCO we performed FMS calculations, using the structure derived from the best fit (see table 1 of the main text) and varied the angle α in steps of two degrees. All non-structural parameters were kept fixed to those of the best fit, according to table S7. As shown in Figs S2 and S3 the variations in the calculated spectra are very subtle, making the assessment of the best value for α difficult.

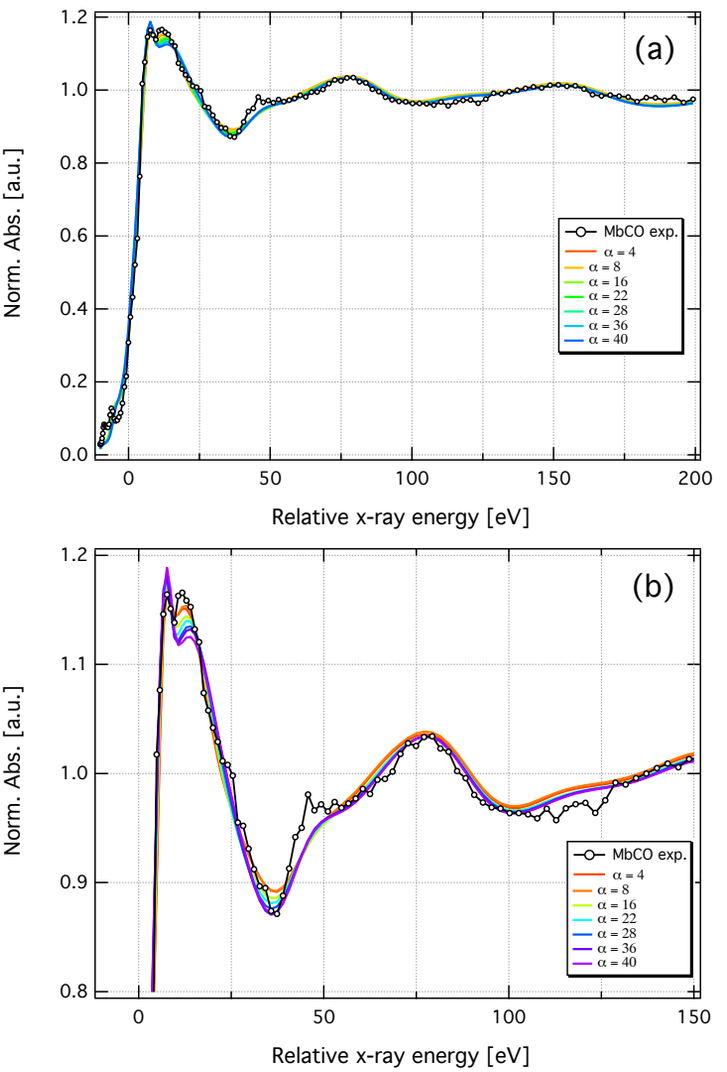

Figure S3: Calculated XAS spectrum of MbCO as a function of the angle α (a). A zoom into the XANES region is shown in (b)

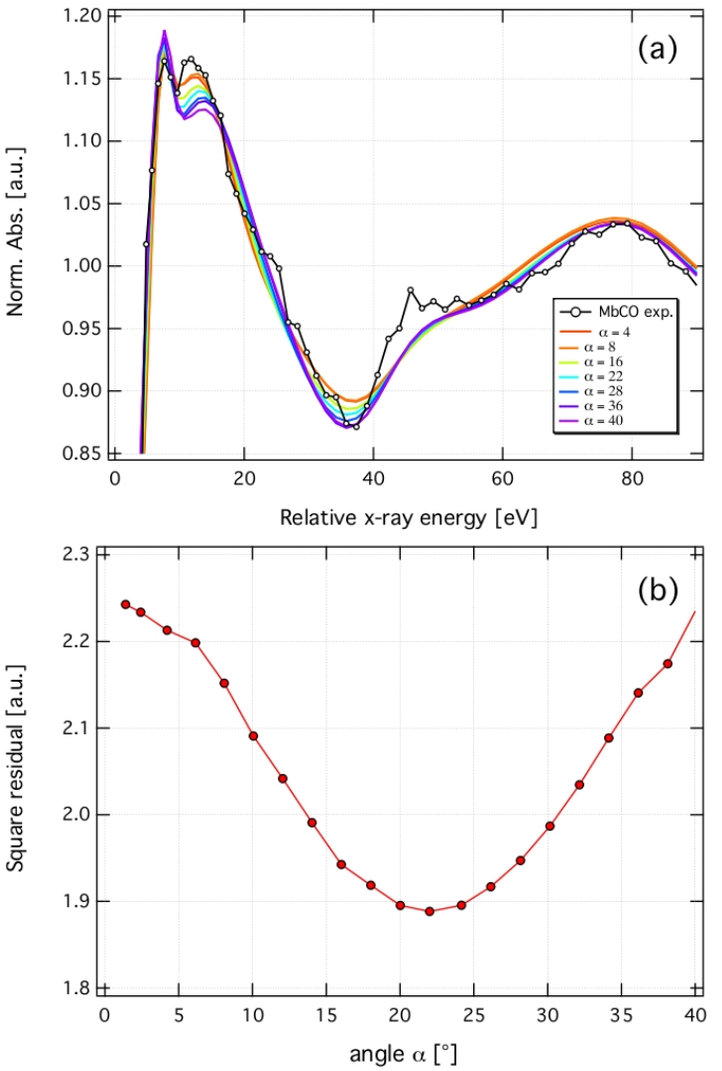

Figure S4: (a) A zoom into the near-edge and the S^2 value (b) for the calculated XAS spectrum of MbCO as a function of the angle α

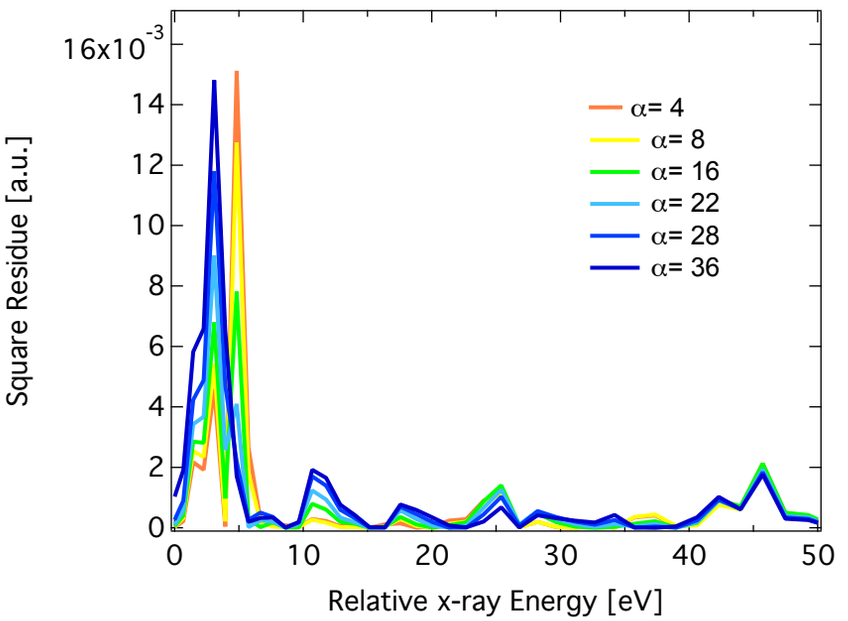

Figure S5: The S^2 value, plotted as a function of energy for the calculated XAS spectrum of MbCO as a function of the angle α

S2.5 Calculated XAS spectrum of MbO_2 as a function of the Fe-O bond length

Using the structure derived from the best fit (see table 3 of main text) we performed FMS calculations using the MXAN package using the the same protocol described in section S2.1 varying the bond length distance in steps of 0.2 Å. All non-structural parameters were kept fixed to those of the best fit. The variations in the calculated spectra are noticeable. For a Fe-O bond length of 1.81 Å the calculated spectrum deviates significantly from the experimental data. This effect is also reflected in the relatively big value for the square residual.

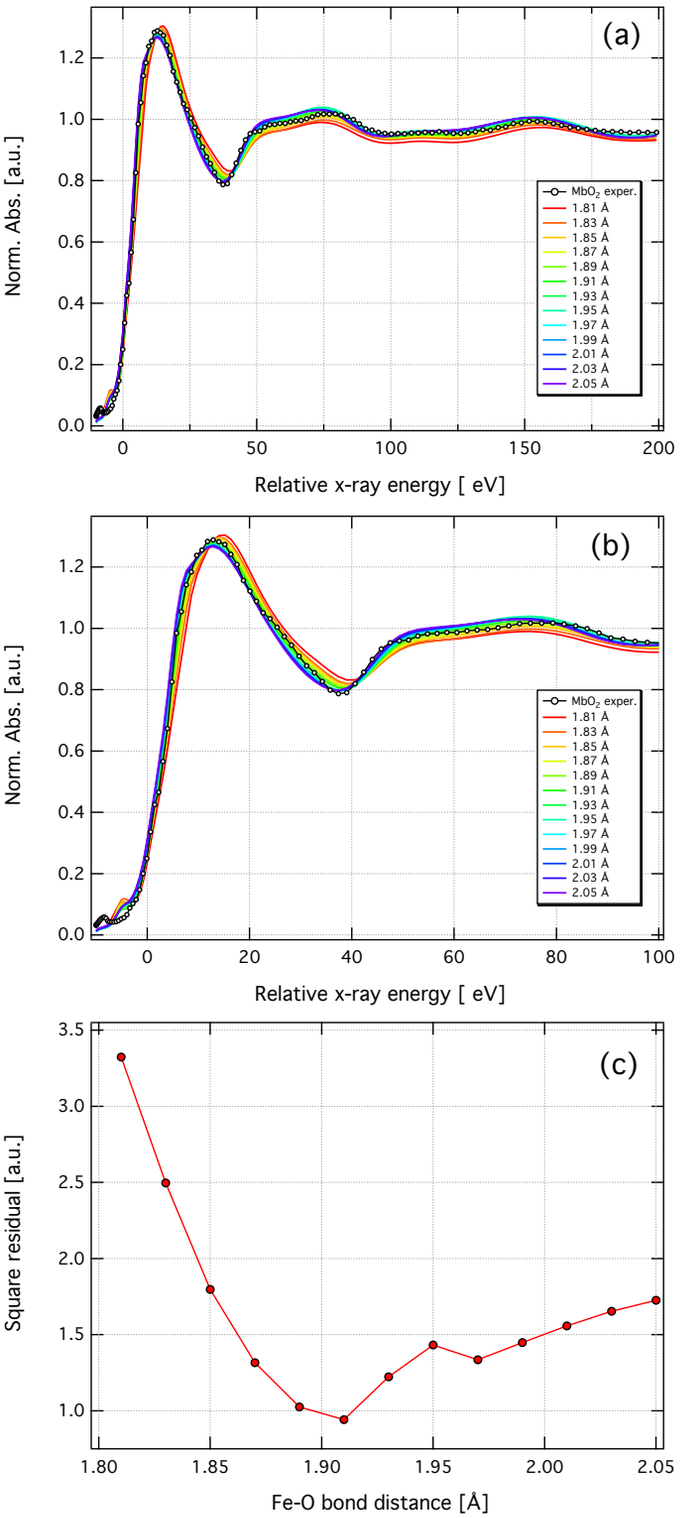

Figure S6: Calculated XAS spectrum of MbO_2 as a function of the Fe-O bond length (a) and zoom in the region around the edge (b). (c) The S^2 value for the difference Fe-O bond lengths.

S2.6 Calculated XAS spectrum of metMb with and without a H_2O molecule

The crystal structure of metMb reports a water molecule in the vicinity of the Fe atom, in a position that would usuaaly be associated with the ligand on other forms of Mb. We placed an oxygen atom in the initial position given by the crystallographic coordinates, bound to a helium atom to simulate the presence of the two hydrogen atoms in the water molecule.

The effect of the presence of a water molecule in the vicinity of the iron atom in the calculated XAS spectrum of metMb was investigated by performing a complete optimization in MXAN with and without the presence of this molecule. The results are shown in figure S7. The absence of the H_2O molecule had little impact in the calculated spectrum. Apart of the small difference in the region around 50 eV, both calculated spectra are equivalent. The square residual increased from $S^2 = 0.57$ when the water molecule is used to $S^2 = 0.99$ when no water is included. Therefore in our description of the structure of metMb we make use of the water as a ligand, in the position given in table 5 of main text.

S2.7 Model Structures used for TDDFT simulations

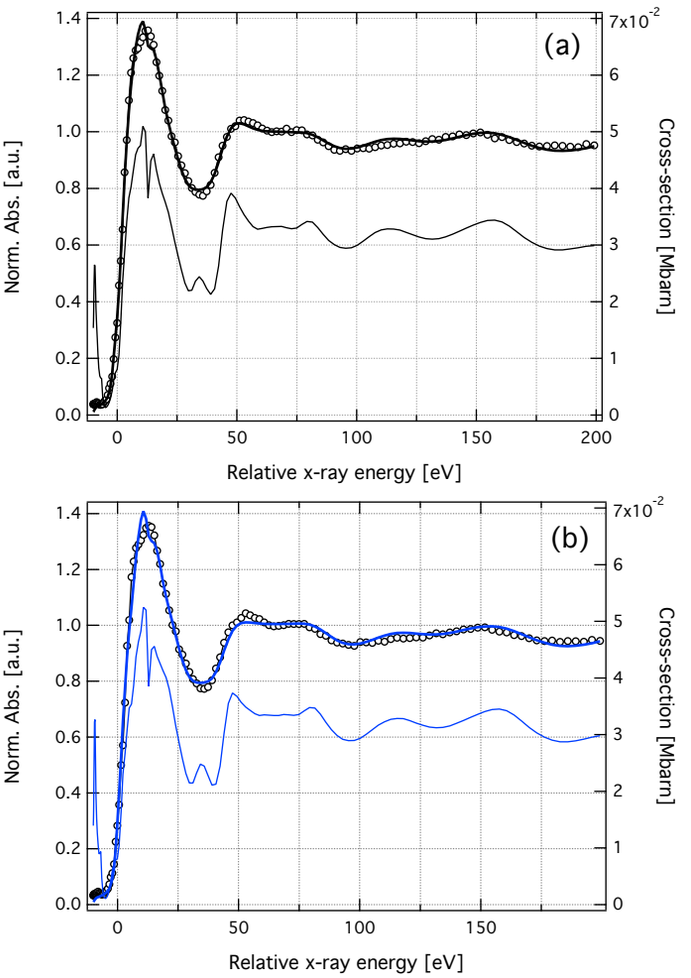

Figure S7: MXAN best fit of the XAS spectrum of metMb with (a) and without (b) a water molecule in the position of the ligand.

	X	Y	Z
Fe	0.000000	0.000000	0.000000
C	-0.053000	-0.593000	-1.731000
N	1.255000	-1.510000	-0.050000
N	-1.532000	-1.297000	-0.003000
N	-1.280000	1.567000	0.018000
N	1.591000	1.279000	0.033000
N	0.066000	0.006000	2.041000
O	-0.088000	-1.060000	-2.740000
C	-0.601000	0.815000	2.812000
C	-2.640000	1.501000	0.076000
C	-2.877000	-1.019000	-0.043000
C	0.965000	-2.899000	-0.237000
C	2.893000	0.983000	0.004000
C	-1.501000	-2.673000	-0.082000
C	2.689000	-1.523000	-0.163000
C	0.706000	-0.844000	2.876000
C	-1.008000	2.933000	0.092000
C	1.535000	2.704000	0.070000
C	-0.316000	-3.354000	-0.186000
C	3.360000	-0.295000	-0.054000
C	-3.357000	0.297000	-0.002000
C	0.324000	3.410000	0.117000
N	-0.409000	0.531000	4.140000
C	0.436000	-0.542000	4.187000
C	-3.195000	2.836000	0.163000
C	-3.669000	-2.190000	-0.167000
C	-2.136000	3.693000	0.143000
C	2.192000	-3.672000	-0.445000
C	3.241000	-2.808000	-0.399000
C	-2.838000	-3.225000	-0.163000
C	3.680000	2.213000	0.042000
C	2.848000	3.239000	0.087000
N	-2.823000	0.472000	-3.496000
C	-3.927000	1.230000	-3.476000
C	-2.561000	0.200000	-4.783000
C	2.150000	-5.119000	-0.786000
C	-5.166000	-2.189000	-0.390000
C	5.168000	2.221000	-0.059000
C	-4.651000	3.189000	0.362000
C	-3.113000	-4.699000	-0.292000
C	4.719000	-3.089000	-0.564000
C	-2.184000	5.217000	0.257000
C	3.141000	4.716000	0.194000
C	0.836000	-1.201000	5.489000
C	-5.523000	-2.123000	-1.904000
C	-4.934000	3.646000	1.819000
C	-3.506000	0.798000	-5.511000
N	-4.351000	1.477000	-4.706000
C	5.896000	3.112000	-0.670000
C	3.170000	-5.892000	-1.020000

Table S2: Model optimised structure of MbCO

	X	Y	Z
Fe	0.000000	0.000000	0.000000
N	0.317000	-0.983000	1.497000
N	-1.378000	1.299000	0.629000
N	1.348000	-1.334000	-0.669000
N	-1.468000	-1.292000	-0.438000
N	1.472000	1.335000	0.392000
N	-0.102000	0.550000	-2.067000
O	0.442000	-2.117000	1.968000
C	-1.022000	1.413000	-2.473000
C	2.704000	-1.163000	-0.574000
C	-1.121000	2.582000	1.085000
C	1.086000	-2.611000	-1.069000
C	1.269000	2.572000	0.985000
C	-1.313000	-2.572000	-0.923000
C	2.827000	1.075000	0.259000
C	-2.814000	-1.103000	-0.221000
C	0.681000	0.205000	-3.142000
C	-2.748000	1.145000	0.638000
C	3.381000	-0.039000	-0.249000
C	-0.138000	-3.171000	-1.258000
C	0.086000	3.180000	1.270000
C	-3.414000	0.030000	0.246000
N	-0.847000	1.638000	-3.768000
C	0.221000	0.887000	-4.220000
C	3.331000	-2.433000	-0.897000
C	2.350000	-3.314000	-1.194000
C	-2.380000	3.247000	1.383000
C	2.556000	3.156000	1.272000
C	-2.620000	-3.182000	-1.041000
C	-3.362000	2.376000	1.113000
C	-3.538000	-2.287000	-0.626000
C	3.593000	2.173000	0.792000
N	0.526000	0.637000	4.270000
C	0.054000	1.839000	4.546000
C	0.707000	-0.053000	5.442000
C	2.446000	-4.825000	-1.607000
C	4.901000	-2.655000	-0.850000
C	0.716000	0.971000	-5.635000
C	-2.529000	4.725000	1.913000
C	-2.879000	-4.649000	-1.547000
C	-4.913000	2.591000	1.273000
C	-5.106000	-2.467000	-0.562000
C	2.897000	4.510000	1.995000
C	5.149000	2.383000	0.908000
N	-0.075000	1.943000	5.856000
C	3.008000	4.199000	3.493000
C	-2.996000	5.572000	0.718000
C	0.323000	0.765000	6.449000
C	-3.723000	-5.476000	-0.896000
C	5.514000	-3.831000	-0.974000

Table S3: Model optimised structure of MbNO.

	X	Y	Z
Fe	0.000000	0.000000	0.000000
O	-0.129000	-0.212000	1.892000
N	-1.334000	1.423000	-0.040000
N	-1.420000	-1.346000	-0.199000
N	1.423000	1.353000	0.487000
N	1.444000	-1.446000	-0.078000
N	0.135000	-0.057000	-2.092000
O	-0.790000	-1.016000	2.496000
C	-1.229000	-2.738000	-0.228000
C	1.251000	2.755000	0.301000
C	-2.797000	-1.182000	-0.158000
C	-1.160000	2.828000	0.149000
C	-2.769000	1.311000	0.067000
C	1.337000	-2.742000	-0.234000
C	1.046000	0.829000	-2.703000
C	2.895000	1.163000	0.254000
C	2.851000	-1.305000	-0.015000
C	-0.617000	-0.673000	-3.066000
C	0.087000	-3.334000	-0.349000
C	0.095000	3.402000	0.245000
C	-3.426000	0.080000	-0.089000
C	3.530000	-0.122000	0.067000
C	2.564000	3.410000	0.281000
C	-3.506000	-2.423000	-0.092000
C	-2.522000	-3.456000	-0.048000
C	3.544000	2.436000	0.261000
C	-0.174000	-0.218000	-4.303000
C	-2.421000	3.562000	0.256000
C	-3.434000	2.585000	0.265000
C	2.558000	-3.480000	-0.157000
N	0.855000	0.729000	-4.138000
C	3.508000	-2.589000	0.008000
N	1.629000	-0.851000	4.129000
C	2.757000	-0.226000	3.810000
C	2.553000	-4.941000	-0.066000
C	-5.009000	-2.458000	0.086000
C	2.786000	4.840000	0.330000
C	-4.890000	2.685000	0.617000
C	5.002000	2.520000	0.268000
C	-2.665000	-4.950000	0.267000
C	-2.539000	5.050000	0.564000
C	-0.642000	-0.651000	-5.700000
C	4.950000	-2.849000	0.367000
C	1.697000	-1.148000	5.504000
N	3.604000	-0.092000	4.954000
C	5.182000	-3.054000	1.853000
C	5.526000	2.989000	-1.111000
C	2.904000	-0.675000	5.961000
C	-5.432000	3.740000	1.405000
C	-3.941000	-5.643000	0.355000

Table S4: Model optimised structure of MbO_2.

	X	Y	Z
Fe	0.000000	0.000000	0.000000
C	0.269000	0.946000	-1.651000
N	-1.339000	-1.322000	-0.685000
N	1.375000	1.293000	0.664000
N	1.459000	-1.267000	-0.499000
N	-1.441000	1.263000	0.561000
N	0.014000	-0.690000	1.938000
N	0.565000	1.601000	-2.498000
C	-0.619000	-1.815000	2.246000
C	1.124000	2.564000	1.091000
C	-1.242000	2.521000	1.073000
C	-2.703000	-1.156000	-0.592000
C	1.261000	-2.493000	-1.150000
C	2.731000	1.183000	0.475000
C	2.827000	-1.020000	-0.397000
C	-2.817000	1.033000	0.378000
C	-1.085000	-2.627000	-1.114000
C	0.747000	-0.294000	3.040000
C	-0.084000	3.159000	1.335000
C	3.422000	0.061000	0.084000
C	-3.445000	-0.093000	-0.124000
C	0.124000	-3.173000	-1.401000
N	-0.345000	-2.124000	3.505000
C	0.565000	-1.226000	4.006000
C	2.375000	3.272000	1.170000
C	3.340000	2.423000	0.789000
C	-3.310000	-2.398000	-1.048000
C	-3.472000	2.216000	0.925000
C	-2.559000	3.116000	1.290000
C	3.543000	-2.121000	-0.988000
C	2.534000	-3.086000	-1.485000
C	-2.356000	-3.278000	-1.405000
N	0.289000	-0.393000	-4.902000
C	-0.279000	-1.588000	-4.989000
C	2.519000	4.768000	1.597000
C	-4.869000	-2.545000	-1.196000
C	-5.055000	2.319000	0.847000
C	-2.790000	4.544000	1.832000
C	4.916000	2.672000	0.632000
C	1.108000	-1.316000	5.406000
C	5.077000	-2.251000	-1.083000
C	2.811000	-4.405000	-2.256000
C	-2.516000	-4.744000	-1.986000
C	0.413000	0.132000	-6.160000
C	2.754000	-4.081000	-3.766000
C	-2.879000	-5.603000	-0.754000
N	-0.490000	-1.865000	-6.268000
C	-3.688000	5.443000	1.347000
C	5.497000	3.846000	0.740000
C	-0.057000	-0.800000	-7.018000

Table S5: Model optimised structure of MbCN.

	X	Y	Z
Fe	0.000000	0.000000	0.000000
N	1.448000	1.308000	0.470000
N	-1.404000	1.289000	0.659000
N	1.397000	-1.326000	-0.674000
N	-1.459000	-1.351000	-0.453000
N	-0.228000	0.796000	-1.981000
C	-1.175000	2.566000	1.157000
C	1.286000	2.537000	1.074000
C	2.746000	-1.184000	-0.537000
C	2.805000	1.119000	0.349000
C	-2.771000	1.115000	0.650000
C	1.173000	-2.619000	-1.093000
C	-1.293000	-2.606000	-0.986000
C	-2.819000	-1.172000	-0.299000
C	-1.003000	1.798000	-2.303000
C	0.449000	0.465000	-3.117000
C	0.055000	3.109000	1.371000
C	3.388000	-0.047000	-0.103000
C	-0.083000	-3.172000	-1.274000
C	-3.408000	-0.034000	0.223000
N	-0.820000	2.137000	-3.588000
C	-2.453000	3.190000	1.428000
C	2.575000	3.110000	1.359000
C	3.519000	2.253000	0.915000
C	2.430000	-3.311000	-1.257000
C	-3.433000	2.308000	1.131000
C	3.402000	-2.442000	-0.885000
C	-3.534000	-2.328000	-0.766000
C	-2.596000	-3.231000	-1.191000
C	0.102000	1.288000	-4.132000
N	0.308000	0.337000	4.360000
C	-0.273000	1.460000	4.676000
C	0.540000	-0.284000	5.575000
C	4.883000	-2.674000	-0.675000
C	5.022000	2.333000	1.049000
C	2.809000	4.366000	2.244000
C	-2.798000	-4.637000	-1.651000
C	2.541000	-4.780000	-1.639000
C	-4.926000	2.465000	1.300000
C	-2.661000	4.609000	1.980000
C	-5.042000	-2.519000	-0.736000
C	0.618000	1.397000	-5.544000
C	-2.161000	5.563000	-0.335000
N	-0.412000	1.570000	6.005000
C	2.958000	4.067000	3.741000
C	-3.131000	5.547000	0.828000
C	0.125000	0.462000	6.581000
C	-3.683000	-5.503000	-1.261000
C	5.556000	-3.759000	-0.888000
O	0.013	-0.227	2.303

Table S6: Model optimised structure of metMb.

	X	Y	Z
Fe	0.000000	0.000000	0.000000
N	-1.628000	1.247000	0.034000
N	-1.282000	-1.630000	-0.122000
N	1.656000	-1.268000	-0.058000
N	1.272000	1.633000	0.034000
N	0.041000	0.106000	2.285000
C	-0.804000	0.802000	3.023000
C	1.591000	-2.623000	-0.336000
C	-0.852000	-2.944000	-0.324000
C	-2.669000	-1.549000	-0.270000
C	2.643000	1.598000	-0.078000
C	-2.955000	0.887000	-0.075000
C	-1.585000	2.638000	-0.007000
C	2.970000	-0.862000	-0.236000
C	0.880000	2.964000	0.016000
C	0.824000	-0.661000	3.112000
C	0.447000	-3.389000	-0.324000
C	-3.424000	-0.402000	-0.178000
C	3.414000	0.447000	-0.128000
C	-0.431000	3.405000	0.031000
N	-0.587000	0.511000	4.294000
C	0.444000	-0.402000	4.383000
N	-1.890000	-0.571000	-3.836000
C	2.938000	-3.096000	-0.631000
C	3.125000	2.968000	-0.093000
C	-3.769000	2.086000	-0.090000
C	-2.947000	3.136000	-0.037000
C	-2.004000	-3.791000	-0.561000
C	3.775000	-2.041000	-0.563000
C	2.068000	3.793000	-0.038000
C	-3.206000	-2.872000	-0.520000
C	-3.169000	-0.276000	-3.696000
C	-1.593000	-0.636000	-5.176000
C	3.239000	-4.590000	-0.856000
C	4.608000	3.345000	-0.115000
C	-3.343000	4.613000	0.063000
C	-5.303000	2.087000	-0.015000
C	0.900000	-0.984000	5.684000
C	5.305000	-2.018000	-0.692000
C	2.048000	5.332000	0.031000
C	-2.027000	-5.314000	-0.736000
C	-4.670000	-3.291000	-0.698000
N	-3.702000	-0.147000	-4.897000
C	-4.867000	-3.404000	-2.217000
C	-5.729000	2.396000	1.433000
C	-2.739000	-0.386000	-5.850000
C	5.055000	4.367000	-0.856000
C	4.462000	-5.037000	-1.134000

Table S7: Model optimised structure of deoxyMb.

References

[1] Daniel Copeland, Alexei Soares, Ann West, and George Richter-Addo. Crystal structures of the nitrite and nitric oxide complexes of horse heart myoglobin. *Journal of inorganic biochemistry*, 100(8):1413–1425, 2006.

[2] Seongheun Kim, Geunyeong Jin, and Manho Lim. Dynamics of geminate recombination of no with myoglobin in aqueous solution probed by femtosecond mid-ir spectroscopy. *Journal of Physical Chemistry B*, 108(52):20366–20375, 2004.

[3] Bruce Ravel and Mathew Newville. Athena, artemis, hephaestus: data analysis for x-ray absorption spectroscopy using ifeffit. *Journal of Synchrotron Radiation*, 12:537–541, 2005.

[4] M Benfatto, C Natoli, A Bianconi, J Garcia, A Marcelli, M Fanfoni, and I Davoli. Multiple-scattering regime and higher-order correlations in x-ray-absorption spectra of liquid solutions. *Physical Review B*, 34(8):5774, Oct 1986.

[5] M Benfatto, A Congiu-Castellano, A Daniele, and S Della Longa. Mxan : a new software procedure to perform geometrical fitting of experimental xanes spectra. *Journal of Synchrotron Radiation*, 8(2):267–269, 2001.

[6] M Benfatto, S Della Longa, and C Natoli. The mxan procedure: a new method for analysing the xanes spectra of metalloproteins to obtain structural quantitative information. *Journal of Synchrotron Radiation*, 10(1):51–57, Jan 2003.

[7] M Benfatto and S Della Longa. Mxan: New improvements for potential and structural refinement. *Journal of Physics: Conference Series*, 190(012031):1–4, Jan 2009.

[8] Joe Norman. Non-empirical versus empirical choices for overlapping-sphere radii ratios in scf-xα-sw calculations on clo4- and so2. *Molecular Physics: An International Journal at the Interface Between Chemistry and Physics*, 31(4):1191–1198, 1976.

[9] C Natoli, M Benfatto, S Della Longa, and K Hatada. X-ray absorption spectroscopy: state-of-the-art analysis. *Journal of Synchrotron Radiation*, 10:26–42, Jan 2003.

[10] J Rehr and R Albers. Theoretical approaches to x-ray absorption fine structure. *Reviews of Modern Physics*, 72(3):621–654, 2000.

[11] Alessandro Arcovito, Chiara Ardiccioni, Michele Cianci, Paola D'Angelo, Beatrice Vallone, and Stefano Della Longa. Polarized x-ray absorption near-edge structure spectroscopy of neuroglobin and myoglobin single crystals. *Journal of Physical Chemistry B*, 114(41):13223–13231, 2010.

[12] Paola D'Angelo, Andrea Lapi, Valentina Migliorati, Alessandro Arcovito, Maurizio Benfatto, Otello Roscioni, Wolfram Meyer-Klaucke, and Stefano Della-Longa. X-ray absorption spectroscopy of hemes and hemeproteins in solution: Multiple scattering analysis. *Inorganic Chemistry*, 47(21):9905–9918, 2008.

[13] S Della-Longa, A Arcovito, M Girasole, J L Hazemann, and M Benfatto. Quantitative analysis of x-ray absorption near edge structure data by a full multiple scattering procedure: The fe-co geometry in photolyzed carbonmonoxy-myoglobin single crystal. *Physical Review Letters*, 87(15):155501, 2001.

[14] A Arcovito, D C Lamb, G U Nienhaus, J L Hazemann, M Benfatto, and S Della Longa. Light-induced relaxation of photolyzed carbonmonoxy myoglobin: A temperature-dependent x-ray absorption near-edge structure (xanes) study. *Biophysical Journal*, 88(4):2954–2964, 2005.

[15] Alessandro Arcovito, Maurizio Benfatto, Michele Cianci, S Samar Hasnain, Karin Nienhaus, G Ulrich Nienhaus, Carmelinda Savino, Richard W Strange, Beatrice Vallone, and Stefano Della Longa. X-ray structure analysis of a metalloprotein with enhanced active-site resolution using in situ x-ray absorption near edge structure spectroscopy. *Proceedings of the National Academy of Sciences*, 104(15):6211–6216, 2007.

[16] L Hedin and B I Lundqvist. Explicit local exchange-correlation potentials. *Journal of Physics C: Solid State Physics*, 4(14):2064–283, 1971.

[17] M Benfatto, J Solera, J Chaboy, M Proietti, and J García. Theoretical analysis of x-ray absorption near-edge structure of transition-metal aqueous complexes in solution at the metal k edge. *Physical Review B*, 56(5):2447, Aug 1997.

[18] M Benfatto and S Della Longa. Geometrical fitting of experimental xanes spectra by a full multiple-scattering procedure. *Journal of Synchrotron Radiation*, 8(4):1087–1094, 2001.

[19] J Rehr. Theory and calculations of x-ray spectra: Xas, xes, xrs, and nrixs. *Radiation Physics and Chemistry*, 75(11):1547–1558, Jan 2006.

[20] K Hayakawa, K Hatada, S Longa, and P Angelo. Progresses in the mxan fitting procedure. *AIP Conference Proceedings - XAFS 13*, Jan 2007.

[21] S Debeer-George, T Petrenko, and Neese F. Time-dependent density functional calculations of ligand K-edge X-ray absorption spectra. *Inorganica Chimica Acta*, 361:965–972, 2008.

[22] S DeBeer-George, T Petrenko, and F Neese. Prediction of Iron K-Edge Absorption Spectra Using Time-Dependent Density Functional Theory. *J. Phys. Chem. A*, 112:12936–12943, 2008.

[23] F. Neese. *Max-Planck-Institut für Bioanorganische Chemie*, 2012. ORCA: an ab initio, Density Functional and Semiempirical program package, Version 2.9.

[24] B. M. Bode and M. S. Gordon. Macmolplt: a graphical user interface for GAMESS. *J. Mol. Graphics Mod.*, 16:133–138, 1998.

[25] J. P Perdew. Density-Functional Approximation for the Correlation-Energy of the Inhomogeneous Electron-Gas. *Physical Review B*, 33:8822–8824, 1986.

[26] A. D. Becke. Density-functional exchange-energy approximation with correct asymptotic behavior. *Phys. Rev. A*, 38:3098–3100, 1988.

[27] M Reiher, O Salomon, and B Artur Hess. Reparameterization of hybrid functionals based on energy differences of states of different multiplicity. *Theoretical Chemistry Accounts*, 107(1):48–55, 2001.

[28] G Capano, TJ Penfold, N Besley, I Tavernelli, CJ Milne, M Reinhard, R Abela, U Rothlisberger, and M Chergui. The role of Hartree-Fock exchange in the simulations of X-ray absorption spectra: A study of photoexcited [Fe(bpy)3]2+. *in preparation.*

[29] S. Hirata and M Head-Gordon. Time-dependent density functional theory within the Tamm-Dancoff approximation. *Chemical Physics Letters*, 314:291–299, 1999.

[30] F Neese. Prediction and interpretation of the 57fe isomer shift in mãssbauer spectra by density functional theory. *Inorganica Chimica Acta*, 337(0):181 – 192, 2002.